Complex phase behaviour from simple potentials

2007 J. Phys.: Condens. Matter 19 073101

(http://iopscience.iop.org/0953-8984/19/7/073101)

INSTITUTE OF PHYSICS PUBLISHING JOURNAL OF PHYSICS: CONDENSED MATTER

J. Phys.: Condens. Matter **19** (2007) 073101 (23pp) doi:10.1088/0953-8984/19/7/073101

TOPICAL REVIEW

Complex phase behaviour from simple potentials

G Malescio

Dipartimento di Fisica, Università di Messina, 98166 Messina, Italy

Received 27 November 2006
Published 15 January 2007
Online at stacks.iop.org/JPhysCM/19/073101

Abstract

Simple pair potentials, where the term 'simple' denotes potentials that are isotropic and refer to one-component systems, can be used to describe effective interactions among substances with supramolecular architecture. By suitably choosing the functional dependence on the intermolecular distance, through such potentials it is possible to take into account, in an average way, the effect of the internal degrees of freedom of the macromolecules. This may give rise to phase phenomena that are radically different from those characterizing typical monoatomic systems. Here we review a number of simple model potentials presenting unusual, i.e. not argon-like, features and discuss the role of attraction and repulsion in determining their phase behaviour.

Contents

1. Introduction

Intermolecular interactions are due to electromagnetic forces between the electrons and the nuclei forming the molecules. Because of the quantum-mechanical character of the motion of these particles, a rigorous theory of intermolecular forces requires the solution of the Schrödinger equation for a system of interacting molecules. A substantial simplification of the problem derives from the fact that the electronic and nuclear motions can be separated. Since electrons have small mass and therefore move much more rapidly than nuclei, the latter can be regarded as being at rest in the zero-order (adiabatic) approximation. The energy associated with the motion of the electrons plays the role of a potential energy for the motion of the nuclei, that may be thus looked upon as occurring in this 'intermolecular' potential [1]. Recent advances in computational techniques have made it possible to describe the interactions

between molecules in considerable detail. In particular, *ab initio* calculations [2] can provide rather accurate information about potential energy surfaces. However, since the computational effort increases in proportion to a high power of the number of electrons, it is impracticable to use these methods for molecules containing more than few atoms. Consequently, the use of models of intermolecular potentials retains its importance for a vast number of applications.

Intermolecular interactions are usually represented in terms of pair potentials, that are to be regarded as effective potentials, taking into account, in some average sense, the contribution of many-body effects. Pairwise additivity is generally assumed, i.e. the total intermolecular potential of N molecules with coordinates r_i ($i = 1, \ldots, N$) is written as

$$U = \sum_{i<j}^{N} u(r_{ij}), \qquad \text{where } r_{ij} = |r_i - r_j|. \tag{1}$$

Pair potentials were originally developed focusing on neutral, chemically inert and approximately spherical molecules, such as rare gases. These systems are modelled through isotropic potentials that depend only on the absolute value of the interparticle distance r.

The essential features of interatomic interaction are the harsh repulsion at short range caused by the overlap of outer electron shells, and the attraction at large separations arising from multipole dispersion interactions, whose leading term, dipole–dipole interaction, varies as r^{-6} [3]. Mainly for mathematical convenience, short-range repulsion is also often represented through an inverse power law. The two behaviours can be incorporated in a single potential function $u(r)$ having the form

$$u(r) = 4\varepsilon \left[(\sigma/r)^{12} - (\sigma/r)^{6} \right], \tag{2}$$

which is the celebrated Lennard-Jones (LJ) potential [4]. In equation (2) ε is the depth of the potential minimum and σ is the separation of the particles at which $u(r) = 0$. The LJ potential provides a remarkably adequate description of the interaction between pairs of rare gas atoms and other approximately spherical molecules such as CH_4. The size and energy parameters appropriate to the different substances may be determined through measurements of physical properties, such as the second virial coefficient.

The LJ potential yields a phase diagram reproducing the behaviour of typical monoatomic substances, with a gas–liquid critical point and a gas–liquid–solid triple point (figure 1). The critical constants, when expressed in reduced units ($T^* = k_B T/\varepsilon$, $\rho^* = \rho\sigma^3$, $P^* = P\sigma^3/\varepsilon$, where k_B is the Boltzmann constant), assume similar values for a remarkable number of substances. This led Johannes van der Waals to propose his law of corresponding states (LCS), according to which, if the thermodynamic variables are scaled with respect to their values at the critical point, all fluids follow the same equation of state and coexistence curve, which amounts to saying that a unique reference system can account for the properties of all fluids [5–7]. Though the validity of LCS is restricted essentially to rare gases, it has proven important for countless applications. The ability of the LJ potential to describe interparticle interactions for a number of important atomic systems, and the remarkable achievements of the LCS, contributed to establishing the concept of an ideal fluid, characterized by argon-like features both as concerns the interparticle interactions and the phase behaviour, as being representative of typical fluids. Therefore, for a long time, scientists, even when investigating model potentials with functional dependence on the interparticle distance that is different with respect to equation (2), were led to choose interaction parameters mimicking the LJ potential, thus obtaining an analogous phase behaviour.

The phase diagram shown in figure 1 can be interpreted in terms of the role played by repulsion and attraction. Over a century ago, van der Waals (vdW) provided a basic explanation of the liquid–gas phase separation and its mechanisms in simple molecular fluids [5, 6]. He

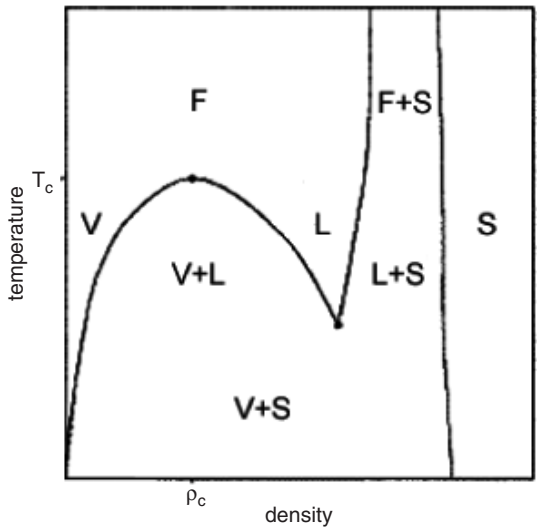

Figure 1. The phase diagram of a typical monoatomic substance, showing the boundaries between solid (S), liquid (L) and vapour (V) phases. The regions where two phases coexist are appropriately labelled (L + S stands for liquid–solid coexistence, etc). T_c and ρ_c are the temperature and the density of the critical point.

modified the ideal-gas equation of state by taking into account two fundamental effects: the presence of a hard core for each molecule, which reduces the volume at the disposal of particles, and the existence of a short-ranged intermolecular attraction, which reduces the pressure P below that of an ideal gas at the same density. He thus obtained the famous vdW equation of state:

$$P = k_B T/(v - b) - a/v^2. \tag{3}$$

Here v is the volume per particle, b is a factor proportional to the molecular volume, $a = 2\pi\varepsilon\delta^3/3$, where ε is the energy of 'pair interaction', and δ is the effective range of attraction. Since equation (3) is obtained by concentrating on the average distribution of particles, it neglects the role of correlations. In general, however, for the fluids of interest the correction due to positional correlations between particles does not change, other than quantitatively, the basic predictions of the theory. The vdW equation is a typical example of mean field theory and thus it becomes exact in the limit of infinitely weak and long-range intermolecular attraction. In spite of its limitations, the vdW equation of state indicates a critical point and condensation by way of a simple model, and provides insight into the mechanism of liquid–gas phase separation as driven by the competition between hard-core repulsion and interparticle attraction.

The idea of representing the impenetrability of the particles of a liquid through the presence of a hard core, used by van der Waals in deriving his equation of state, proved crucial also to understanding the relation between interatomic interactions and crystallization. A long-debated question concerned the fate of the freezing transition in the case that all attractions between particles could be switched off. The simplest way of representing purely repulsive interactions is through the hard-sphere potential:

$$u(r) = \begin{cases} 0 & r < \sigma \\ \infty & r > \sigma. \end{cases} \tag{4}$$

The phase behaviour of a system of hard spheres was first addressed systematically by computer

simulations [8, 9]. Rather unexpectedly, it was found that no attraction is needed for freezing. The system in the liquid state reaches the freezing point at a packing fraction $\eta \approx 0.494$, where $\eta = \frac{\pi}{6}\rho\sigma^3$ is defined as the ratio of the volume occupied by the spheres to the total volume. At this point the phase diagram splits into metastable and stable branches. The metastable liquid branch ends at $\eta \approx 0.64$, which corresponds to the random close packing state, that provides the maximum packing fraction that can be achieved by a disordered arrangement. The stable branch, on which liquid and crystal phases coexist, ends at the melting point $\eta \approx 0.545$. Above the melting point, the stable crystal branch is present up to $\eta \approx 0.74$, which corresponds either to the close-packed face centred cubic (fcc) or to the hexagonal close-packed configurations.

A crystal phase formed by hard spheres has a higher entropy than the liquid phase at the same density. Thus, self-ordering into crystalline structures at sufficiently high densities is induced by entropy, which favours more effective packing since this leaves more space for particle fluctuations around their equilibrium positions. Though this result appeared at first somewhat counterintuitive, it was subsequently confirmed through experiments on hard-core colloids [10, 11]. Moreover, calculations showed that, at least at high densities, the structure of a hard-sphere fluid does not differ significantly from that corresponding to more complicated potentials (as, for example, the LJ potential). The structure of dense liquids is largely determined by excluded volume effects, the attractive part of the intermolecular potential playing only a minor role [3].

Starting from the early 1990s, the interest in new materials such as fullerenes and soft matter (colloidal systems, polymers, surfactants, etc) led to exploring the phase behaviour of potentials with features differing from typical argon-like interactions. Model potentials devoid of obvious physical meaning in the context of microscopic interactions of atomic systems become physically relevant when assumed to represent interactions among macromolecules. Due to their molecular architecture, such substances present internal degrees of freedom, that can be accounted for in an average way by effective interaction potentials. Even apparently small deviations of the potential from the LJ form may yield surprising changes in the phase diagram.

This review is organized as follows. In sections 2–4 we examine how unusual phase behaviours may emerge when the intermolecular potential departs from the typical argon-like form. For ease of presentation we will consider first the attractive component of the potential (section 2), then we will consider potentials with diverging repulsion (section 3) and bounded repulsion (section 4). Finally, in section 5 we present concluding remarks.

2. Attraction

As first pointed out by the vdW equation of state, the presence of attraction is necessary in order that condensation occurs and thus the liquid phase may exist. However, the existence of the liquid phase depends crucially on the features of the attractive intermolecular forces. Above a substance's liquid–vapour critical point the distinction between the liquid and vapour phases disappears. Below the triple point, at which solid, liquid and vapour coexist, only the solid and vapour phase are stable. The liquid range is thus bounded below by the triple point temperature T_t, and above by the critical point temperature T_c. The ratio $R = T_c/T_t$ provides an approximate measure of the extension of the liquid region. As shown in table 1, for the rare gases R is approximately 1.8. The value of R depends on the nature of the intermolecular forces and varies with the relative importance of attractive and repulsive forces. For the LJ potential, $R \approx 1.96$, not far away from that of rare gases.

The overall attraction strength depends on the well depth as well as on the attractive range. Varying the well depth amounts to redefining the energy unit. This essentially causes a rescaling

Table 1. Values of $R = T_c/T_t$ for rare gases (T_c and T_t are, respectively, the critical point and the triple point temperature).

Gas	R
Ar	1.801
Xe	1.796
Ne	1.807
Kr	1.809

of the temperatures in the phase diagram, which does not qualitatively alter its main features. On the contrary, changing the range of the attractive part of the intermolecular potential may have dramatic effects on the phase behaviour. As discussed in section 1, condensation arises from the competition between core repulsion and interparticle attraction. For most molecular substances, the ratio of the ranges of the attractive and repulsive interactions is such that a liquid–vapour transition is to be expected. In particular, this holds true for particles interacting through a pair potential that can be approximated by the Lennard-Jones potential [12]. The situation may be considerably different for macromolecules, where effective interactions can have a rather small attractive range. In such conditions the liquid phase may be no longer stable. This observation was first made in the context of colloid science [13–15]. Mesoscopic colloidal particles immersed in a fluid of smaller particles experience the entropically induced depletion interaction. This is an attractive interaction arising from the presence of a smaller species, such as polymer molecules, micelles, or other nanoparticles, in a suspension of colloidal particles. As the particles come close together, the polymers no longer penetrate the region in between the two particles. As a result, the osmotic pressure is unbalanced and drives the two particles closer together. Thus a net attractive force is set up between the particles [14]. Quite remarkably, the features of the depletion interaction can be opportunely tuned [16, 17]. For example, in colloid–polymer mixtures the attractive depletion potential can be tuned by varying the polymer concentration and the colloid–polymer size ratio. This makes it possible to vary the range of the attraction between particles and thus investigate the effect of such variation on their phase behaviour. Computer simulations [18], theoretical work [19] and experiments [20, 21] indicated that the colloidal liquid–vapour transition disappears for sufficiently short-ranged attractive interactions between the colloidal particles. In particular, the liquid phase appears to be stable if the range of attraction is greater than about 20–30% of the particle diameter.

As it concerns molecular fluids, the issue was first investigated in relation to the behaviour of C_{60} and the possible existence of a liquid phase of this molecule. Although C_{60} is a fairly inert, essentially spherical molecule, intermolecular interactions are not argon-like. A simple pair potential proposed to describe C_{60}–C_{60} intermolecular interaction is the Girifalco potential [22]. This was derived by considering C_{60} molecules as perfect spheres with a surface consisting of a uniform density of carbon atoms. The carbon atoms of two different C_{60} molecules are assumed to interact through the LJ potential. At high temperatures interactions can be averaged over all relative orientations of the C_{60} molecule, thus obtaining the isotropic intermolecular potential

$$\phi = -\alpha\left[\frac{1}{s(s-1)^3} + \frac{1}{s(s+1)^3} - \frac{2}{s^4}\right] + \beta\left[\frac{1}{s(s-1)^9} + \frac{1}{s(s+1)^9} - \frac{2}{s^{10}}\right] \tag{5}$$

where $s = r/2a$, r being the distance between the centres of the two interacting C_{60} molecules and a their radius, 3.55 Å, and α and β are empirical parameters whose values are determined from the heat of sublimation and lattice constant of fcc fullerite. The Girifalco potential is characterized by an attractive range that is significantly shorter with respect to the LJ potential

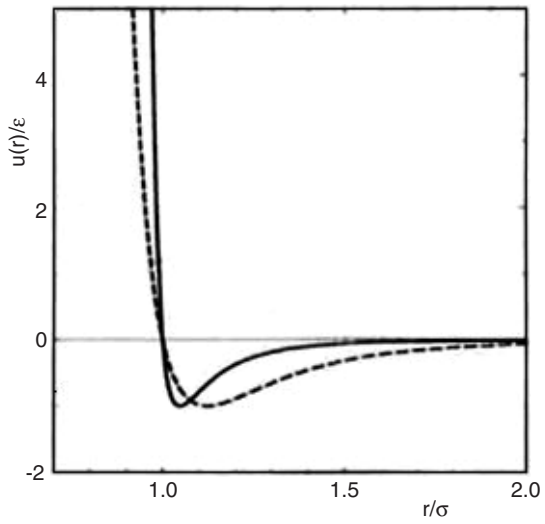

Figure 2. Lennard-Jones (dashed line) and Girifalco (solid line) potentials. ε is the well depth and σ is the effective diameter, defined as the distance where $u(r) = 0$.

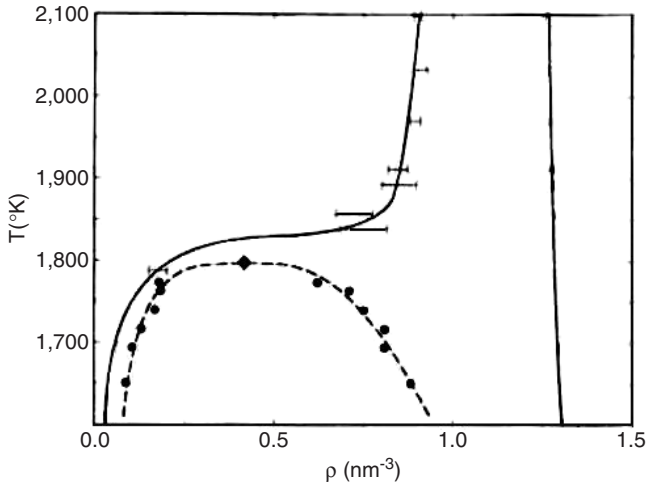

Figure 3. Temperature–density phase diagram for a system of particles interacting through the Girifalco potential, as reported in [23]. Solid and dashed lines are, respectively, the solid–fluid and the metastable liquid–vapour coexistence lines, derived by a fit to the data points obtained through free energy calculation (solid lines) and Monte Carlo Gibbs-ensemble simulation technique (dashed line). The solid diamond indicates the estimated location of the critical point.

(figure 2). This is because the carbon–carbon interaction determines the range of the attractive tail, whereas the diameter of the repulsive core is fixed by the size of the C_{60} cage.

The phase diagram of C_{60} was investigated through computer simulation using the Girifalco potential to describe intermolecular interactions. Through Monte Carlo (MC) calculations it was found that the sublimation line passes above the metastable liquid–vapour coexistence curve and thus no stable liquid phase exists [23] (figure 3). Molecular dynamics (MD) predicted instead the existence of a liquid phase, though in a temperature range much

narrower with respect to the LJ potential [24]. A partial explanation for the discrepancy between such results is presumably to be found in the method adopted to treat the long-range tail of the potential [25]. More recently, a study based on MC simulation showed the existence of a narrow stable liquid phase for this system [26]. Since the temperature range of the critical point (∼1800 K) is above the temperature at which C_{60} has been reported to polymerize [27], an experimental assessment of the liquid phase of C_{60} remains difficult to perform. However, the above studies made clear that the existence of the liquid phase is strictly related to the range of the attractive intermolecular forces. To better understand this relationship a number of model systems with variable attractive range have been investigated. We will review some of them.

A systematic study of the relation between the range of the attractive part of the intermolecular potential and the stability of the liquid phase was performed for a model fluid interacting through hard-sphere repulsion with an attractive Yukawa tail of variable range [28]:

$$u(r) = \begin{cases} \infty & r < \sigma \\ -\varepsilon \dfrac{\exp\left[\kappa\sigma(1 - r/\sigma)\right]}{r/\sigma} & r \geqslant \sigma \end{cases} \tag{6}$$

where σ is the diameter of the hard core, ε is the well depth, and $1/\kappa$ is a measure of the range of the attractive part of the potential. Calculations performed for various values of κ, using Monte Carlo simulation and perturbation theory, showed that the liquid–vapour coexistence curve disappears below the sublimation line when the range of the attractive part of the Yukawa potential is less than approximately one-sixth of the hard-core diameter.

A model system with variable attractive range, and allowing for analytical free energy calculations, consists in particles interacting through a potential described by a double Yukawa functional form [29]:

$$u(r) = \varepsilon\phi(r), \qquad \phi(x) = \frac{c}{x}\left(\mathrm{e}^{-a(x-1)} - \mathrm{e}^{-b(x-1)}\right), \tag{7}$$

where $a > b$, ε fixes the energy scale, $x = r/\sigma$ and $r = \sigma$ is the zero of $u(r)$. The dimensionless parameters a, b, c determine, respectively, the steepness of the repulsion, the range of attraction and the well depth. By assuming a constant well depth, the potential can be parameterized by (a, b) or equivalently by the position x_0 of the minimum of $\phi(x)$ and the value x_1 for which $\phi(x)$ has dropped to 1% of its value at the minimum. Thus, $x_1 - x_0$ is a measure of the attractive range. The phase diagram of the potential described by equation (7), calculated through a variational method, transforms, by progressively reducing the range of attraction, from the usual type, with a fluid–fluid critical point and a fluid–fluid–solid triple point (figure 4(a)), to a phase diagram where the liquid–vapour coexistence curve is metastable with respect to the sublimation line and thus no stable liquid phase exists (figure 4(b)). By further reducing the attractive range, another remarkable change occurs in the phase diagram: it becomes a fluid–solid mirror image of the argon-like phase diagram, with a solid–solid critical point and a solid–solid–fluid triple point (figure 4(c)). Thus, when one does allow for extremely short-ranged attraction the phase diagram exhibits a fluid–solid symmetry.

Among the model potentials most widely used in statistical mechanics, an important place is occupied by that consisting in hard-sphere repulsion plus a square well:

$$u(r) = \begin{cases} \infty & 0 \leqslant r < \sigma \\ -\varepsilon & \sigma \leqslant r < \sigma + \delta \\ 0 & r \geqslant \sigma + \delta. \end{cases} \tag{8}$$

This model, called the HSSW (hard-sphere square-well) fluid, has two intrinsic length scales: the hard-core diameter σ and the width δ of the attractive well; and it allows for an unambiguous

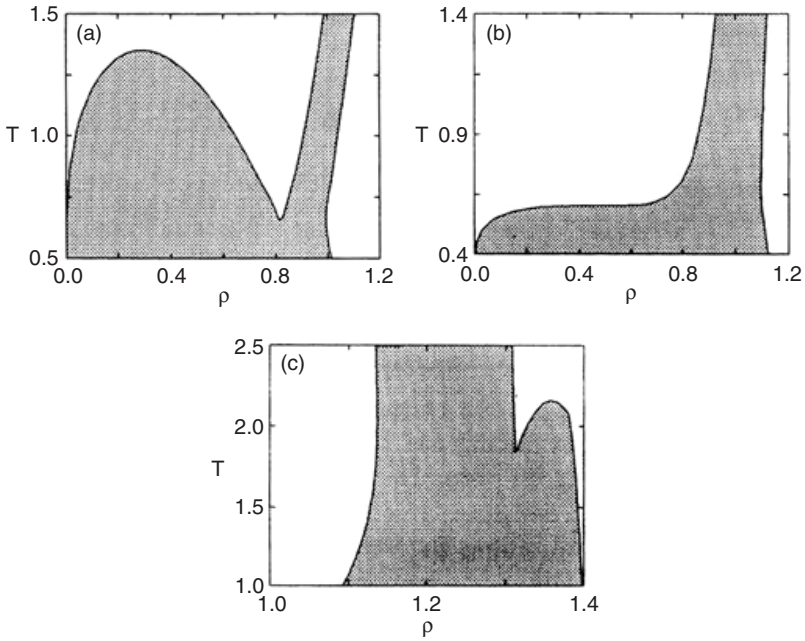

Figure 4. The phase diagram in the temperature (T) and density (ρ) plane (in units such that $\sigma = \varepsilon = k_B = 1$) for a fluid interacting through the potential in equation (7). Panel (a): fit of equation (7) to a LJ potential, $x_1 \approx 2.62$ and $x_0 \approx 1.12$. Panel (b): $x_1 \approx 1.51$ and $x_0 \approx 1.07$, just below the threshold ($x_1 \approx 1.6$) for the disappearance of the liquid phase. Panel (c): $x_1 \approx 1.019$ and $x_0 \approx 1.0025$, just below the threshold ($x_1 \approx 1.05$) for the appearance of an isostructural solid–solid transition. Data are from [29].

definition of the range of the attractive interaction. The ratio of these lengths determines the phase behaviour. The behaviour of this model reduces to the van der Waals fluid in the case of a wide and shallow well ($\delta \to \infty$), while it coincides with sticky or adhesive spheres for $\delta \to 0$. Both of these 'limiting' models depend on one parameter only.

In the adhesive hard-sphere model the attraction takes the form of an adhesive interaction when particles are actually in contact, and therefore has an effectively infinitesimal range. It can be represented by the pair potential

$$u(r)/k_B T = \begin{cases} \infty & 0 \leqslant r < \sigma \\ \ln\left[12\tau\left(1 - \dfrac{\sigma}{\sigma+\delta}\right)\right] & \sigma \leqslant r < \sigma + \delta \\ 0 & r \geqslant \sigma + \delta, \end{cases} \tag{9}$$

where τ controls the well depth. In the limit $\delta \to 0$, equation (9) describes a hard core of diameter σ surrounded by a square well of infinitesimal width and infinite depth. An analytic equation of state, derived using the Percus–Yevick compressibility equation, shows that the model possesses a critical point below which gas–liquid equilibrium may be observed [30]. This finding was not confirmed by calculations based on the Percus–Yevick equation of state derived from the energy equation [31]. The surface adhesion gives rise to clusters as connected sets of mutually touching particles. Above a temperature-dependent density threshold, clusters percolate, i.e. tend to aggregate into amorphous macroscopic structures that span the whole sample [32]. Recently, the phase behaviour of the adhesive hard-sphere fluid has been

Table 2. Critical point temperature T_c, critical density ρ_c, triple point temperature T_t, and $R = T_c/T_t$, for several values of the attractive range γ, for the potential described in equation (10). Temperature and density are expressed in reduced units. The acronyms MC and PT II stand for Monte Carlo and second-order perturbative theory, respectively. Data are extracted from [36].

γ	T_c	ρ_c	T_t	R	Method
0.1	11.452	0.247	5.589	2.05	MC
1	1.372	0.299	0.830	1.65	MC
3	0.597	0.376	0.500	1.19	MC
4	0.534	0.481	0.494	1.08	PT II
5	0.482	0.518	0.473	1.02	PT II
6	0.445	0.538			PT II

determined using specialized Monte Carlo simulations [33]. The critical point for the fluid–fluid phase transition is found to lie well within the percolated regime, which, at least as far as the phase coexistence curve is concerned, places the Percus–Yevick energy equation closer to the truth with respect to the compressibility equation. In an experimental system with very short-range attractive forces, the onset of infinite clusters might therefore interfere with equilibrium phase separation and critical behaviour.

The HSSW fluid has been used as a model to investigate the effects of a variable attractive range. Its phase behaviour has been determined through Gibbs-ensemble Monte Carlo simulations combined with the aggregation volume-biased method [34], for $\delta = 1.5$, 1.25, and 1.15 (in units of σ). Results, in quantitative agreement with more indirect simulations, conclusively illustrate that in the vicinity of $\delta = 1.25$ vapour–liquid coexistence becomes unstable and the triple point disappears. For $\delta = 1.15$, the vapour–liquid coexistence curve is strongly metastable relative to fluid–solid equilibrium. The HSSW with an extremely short, but finite, attractive range (δ ranging between 0.02 and 0.001 in units of σ) was investigated through Monte Carlo simulation [35]. It was shown that the system undergoes a first-order transition from a dense to a more expanded solid phase with the same structure. Similarly to the results of [28], the solid–solid transition terminates in a critical point. When δ becomes large, the solid–solid transition disappears because it will be preempted by the melting transition.

We conclude this section dedicated to the effect on the phase behaviour of variable attractive range, by considering a system of particles interacting through hard-sphere repulsion plus an inverse power attractive tail:

$$u(r) = \begin{cases} \infty & r < \sigma \\ -\varepsilon \left(\dfrac{\sigma}{r}\right)^{3+\gamma} & r \geqslant \sigma. \end{cases} \tag{10}$$

A systematic investigation of this model was performed using Monte Carlo simulation and second-order perturbative theory [36]. The results indicate that the vapour–liquid transition becomes metastable with respect to freezing when $\gamma > 5$ (see table 2), in broad agreement with results for the hard-sphere attractive Yukawa system commonly used to model colloidal particles, globular proteins and nanoparticles. As the attractive range decreases, one observes, in addition to the obvious decrease of T_c due to the overall reduction of the attraction strength, a shift of the critical density ρ_c towards higher values. In order that condensation occurs, in fact, an adequate number of particles should be involved; thus a higher density is necessary to compensate for the reduced attractive range.

3. Diverging repulsion

Due to the harsh repulsion at short intermolecular distance, the interaction potential $u(r)$ of atomic systems is assumed to diverge as r tends to zero. The simplest potential exhibiting this behaviour is the hard-sphere potential. More realistically, repulsion can be assumed to increase gradually as particles approach each other. Thus, if $u(r)$ diverges for $r \to 0$, in a region around $r = 0$, $u(r)$ is necessarily a convex function of r. This behaviour is usually extrapolated at all values of r, and the repulsive component of the potential is represented through a convex function. A model widely used to describe repulsive interaction is represented by inverse power potentials. This defines a system of 'soft' spheres:

$$u(r) = \varepsilon(\sigma/r)^n, \tag{11}$$

where ε, σ and n are model parameters. The thermodynamic behaviour of this model exhibits scaling properties which result from the dependence of the potential on the single group ($\varepsilon\sigma^n$), so the entire phase diagram, for given n, can be extracted from a single coexistence datum. The parameter n controls the steepness and the range of the interparticle repulsion. As n increases, the potential becomes increasingly hard and short ranged, approaching the hard-sphere limit for $n \to \infty$. On the contrary, as n diminishes, the repulsion becomes increasingly soft and long ranged. For $n = 1$ the classical one-component plasma (OCP) interaction is recovered.

This model is useful in investigating the role of molecular repulsion in freezing. For large n, the system crystallizes into a close-packed structure, usually face-centred cubic (fcc), while the body-centred cubic (bcc) structure is unstable with respect to shear. At $n = 7$ the bcc phase becomes mechanically stable. At intermediate n, fcc is the lowest-energy structure, while bcc retains the higher entropy. Thus, as the temperature is raised from zero, an fcc–bcc polymorphic transition may precede the transition to the fluid (this behaviour is observed in alkali metals and iron). To understand how the crystal structure depends on the repulsion softness, the crystallization of soft spheres was investigated through computer simulation. The phase diagram for the inverse sixth power potential was calculated via molecular dynamics computer simulation [37]. The crystal phase at freezing was found to be bcc. The region of stability of this phase is, however, relatively narrow and the system undergoes a bcc–fcc transition at densities only slightly higher than the freezing point. The solid–fluid coexistence line of soft spheres was determined through Monte Carlo simulation, combined with the Gibbs–Duhem integration technique, for values of the softness s ($s = 1/n$) ranging from $s = 0$ (hard spheres) to $s = 0.25$ [38]. It was found that fcc is the stable crystal form for $s < 0.16$ ($n > 6.25$), while bcc is stable for softer potentials. For $n = 6$ the bcc-fluid and the metastable fcc-fluid are very narrowly separated.

The Yukawa potential is used to model intermolecular interactions in a wide range of physical systems. Among these are colloidal suspensions which consist of charged mesoscopic colloidal particles in a solvent with counterions. The latter screen the interparticle Coulomb interaction. The interactions between these mesoscopic particles are described by the Poisson–Boltzmann equation. The solution of the linearized (Debye–Hückel) approximation, assuming zero particle size, yields the Yukawa potential:

$$u(r) = \varepsilon\frac{\exp(-\kappa r)}{r}, \tag{12}$$

where $1/\kappa$ is a measure of the screening length. This potential exhibits a variety of different shapes: for κ very small it approaches the Coulomb potential, whereas for κ very large it becomes an almost hard-sphere-like potential. The phase diagram of the Yukawa potential was studied through molecular dynamics and Monte Carlo simulation [39–42] and the fluid–solid and solid–solid phase boundaries were obtained as functions of the screening parameter

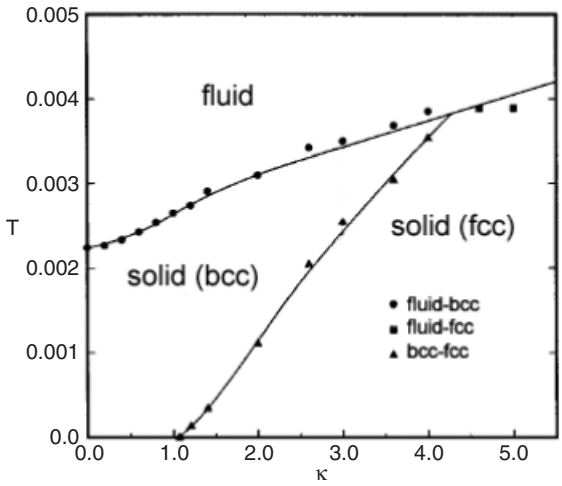

Figure 5. The phase diagram in the (κ, T) plane of the Yukawa system defined by equation (12). Temperature is normalized to the phonon energy of the fcc Yukawa lattice. Solid lines are curves fitted to data points. Data are from [42].

κ [41, 42] (figure 5). At small values of κ (softer repulsion) the fluid crystallizes into a bcc solid, whereas at large κ (steeper repulsion) it crystallizes into an fcc structure. The fluid–solid phase transition and the bcc–fcc phase transition are found to be first order. The solid–solid coexistence line meets the fluid–solid phase boundary in a fluid–solid–solid triple point at $\kappa \approx 4.28$.

The softnest repulsion that can be represented through the inverse power and the Yukawa potentials, diverges, as r approaches zero, as $1/r$. Effective interactions in systems such as star polymers in a good solvent are characterized by an even softer repulsion [43, 44]. To model such interaction a repulsive pair potential which is logarithmic in r inside the core and vanishes exponentially outside the core has been proposed [45]:

$$u(r) = \frac{5}{18} k_{\mathrm{B}} T f^{3/2} \begin{cases} -\ln\left(\dfrac{r}{\sigma}\right) + \dfrac{1}{1+\sqrt{f}/2} & r \leqslant \sigma \\ \dfrac{\sigma}{1+\sqrt{f}/2} \dfrac{\exp\left[-\sqrt{f}(r-\sigma)/2\sigma\right]}{r} & r > \sigma. \end{cases} \tag{13}$$

Constants are chosen such that both the potential and its first derivative are continuous at $r = \sigma$. The parameter f represents the star arm number, i.e., the number of polymer chains tethered to the central particle, while the corona diameter σ measures the spatial extension of the monomer density around a single star centre. The function $\log(r)$ diverges, as r tends to zero, more slowly than any power of r, which justifies the term 'ultrasoft' with which this potential has been defined. Because of the purely entropic origin of the star–star repulsion, the strength of the pair potential in equation (13) scales linearly with $k_{\mathrm{B}}T$, causing the temperature to be an irrelevant thermodynamic quantity. Thus, for the calculation of the phase diagram, only the packing fraction of the stars and the arm number f matter, the latter playing the role of a sort of effective inverse temperature. The phase behaviour of the model system described by equation (13) has been calculated through Monte Carlo simulation and the Rogers–Young integral theory [46] (figure 6).

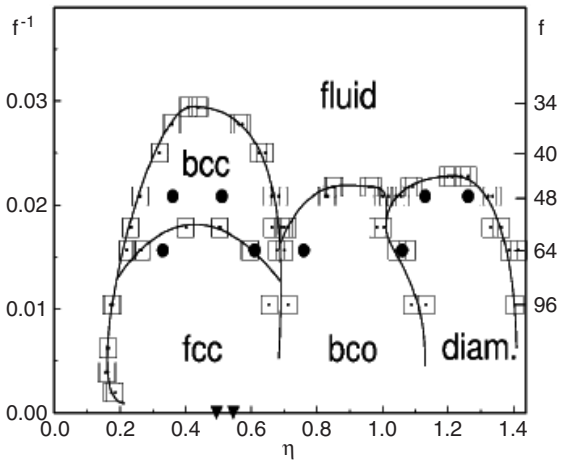

Figure 6. The phase diagram of star polymer solutions with star–star interaction potential defined by equation (13), for different arm numbers f versus the packing fraction η. Squares and circles indicate the phase boundaries obtained by computer simulation and theory, respectively. Lines are guides to the eye. The triangles indicate the freezing and melting point of hard spheres, corresponding to $f \to \infty$. Data are from [46].

For $f \leqslant 34$ the fluid phase is stable for all densities and no crystallization occurs, while for larger f the phase diagram exhibits various solid phases with regions of reentrant melting. Among the stable solid phases are bcc, fcc, body-centred orthogonal (bco), and diamond crystals. The stability of bco and diamond structures is usually related to the presence of anisotropic or three-body forces [47–49]; thus it is rather unexpected for a radially symmetric pair potential. Indeed, the occurrence of such phases stems from the peculiar form of the potential, with a weak divergence for small r and a rapid decrease for $r > \sigma$. This allows the strong interpenetration of the particle coronas along one of the lattice axes, as it follows from the anisotropy of the elementary cell.

The interpretation of f^{-1} as an effective temperature might lead one to conclude that the melting line associated with the potential defined by equation (13) is characterized by the presence of a maximum (and several secondary maxima). Actually, since f is a parameter that enters directly into the functional form of the potential, and not only as a multiplicative constant, the phase diagram of figure 6 should be analysed at fixed f, in order to allow a homogeneous comparison with the other phase diagrams shown in this review. Let us consider, for example, the potential corresponding to $f = 40$. Since the temperature appears in equation (13) as a multiplicative constant, the phase diagram depends solely on the packing fraction η (similarly to hard spheres) and presents a fluid phase for $\eta < \eta_1$, a solid bcc phase for $\eta_1 < \eta < \eta_2$, and a fluid phase for $\eta > \eta_2$, with $\eta_1 \approx 0.25$ and $\eta_2 \approx 0.6$. Thus, the phase diagram presents a reentrant melting with increasing density, but obviously the melting line has no temperature maximum.

Though differing in their softness, all the repulsive potentials considered up to now are convex functions of r. A number of physical systems are characterized by the presence of a penetrable corona surrounding a substantially impenetrable core. Such core–corona molecular architectures can be modelled by a hard-core repulsion plus a finite repulsive shoulder. Thus the functional form that defines the potential presents a region, lying at intermediate distances, with a more or less evident downward concavity. Such potentials, introduced in the early 1970s [50, 51], are often called 'softened' or 'shouldered' potentials and are characterized

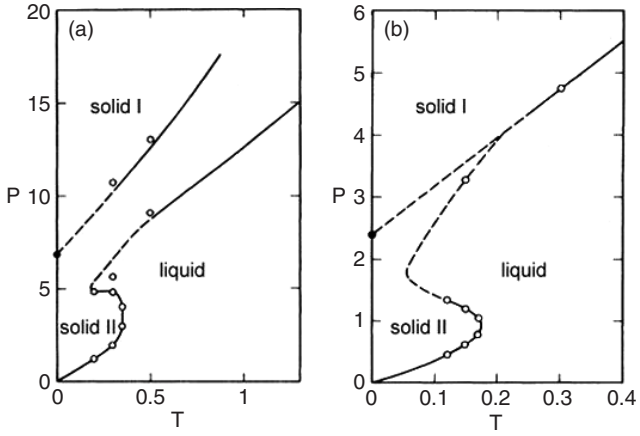

Figure 7. The phase diagram for a 2D system interacting through the potential defined by equation (14): (a) $\delta = 0.2\sigma$; (b) $\delta = 0.5\sigma$. Circles indicate simulation data points. Solid curves represent phase boundaries obtained by perturbation theory. Dashed lines indicate uncertain phase boundaries. Pressure and temperature are in reduced units. Data are from [52].

by the fact that the repulsive force $F(r) = -\mathrm{d}u(r)/\mathrm{d}r$ has, in addition to the maximum at $r = 0$, a secondary maximum, that corresponds to the external shell of the soft penetrable corona.

Softened potentials were first used to model interparticle interactions in cesium and cerium, whose phase behaviour is characterized by a melting line with maxima and minima, and by the presence of solid–solid transitions. Through molecular dynamics and perturbation theory the phase diagram was calculated [52] for a two-dimensional (2D) system of particles interacting through the potential:

$$u(r) = \begin{cases} \infty & 0 \leqslant r < \sigma \\ \varepsilon & \sigma \leqslant r < \sigma + \delta \\ 0 & r \geqslant \sigma + \delta, \end{cases} \tag{14}$$

where σ is the particle diameter and ε is the height of the repulsive shoulder. The phase diagrams obtained show isostructural solid–solid phase transitions and melting-curve extrema (figure 7). The solid–solid transition may end in a critical point or may intersect the melting line in a liquid–solid–solid triple point. These features, similar to those shown by real systems, are related to the presence of the penetrable shoulder. At low temperatures ($k_\mathrm{B}T \ll \varepsilon$) and pressures the particles have effective diameter $\sigma + \delta$, while at high temperatures and pressures the particles have effective diameter σ. Between these two regimes there is a thermodynamic region where the two effective diameters compete with each other, which can lead to phase transitions similar to those characterizing Cs and Ce.

The phase behaviour of the potential described in equation (14) was studied focusing on a relatively short-ranged shoulder potential using perturbation theory [53] and Monte Carlo simulations [54]. Such short-ranged repulsive interactions may occur in a variety of colloidal and macromolecular systems. A possible example is a colloid that is sterically stabilized by partly interpenetrable layers of grafted chain molecules. In analogy to systems with a short-ranged attractive interaction, the shoulder potential leads to an isostructural solid–solid phase transition (figure 8). Extrapolation of the critical density to larger values of δ leads to the estimate that the solid–solid transition will become metastable with respect to the fluid–solid

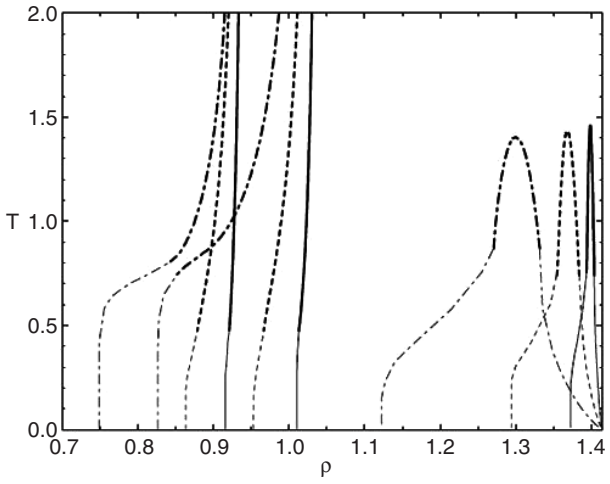

Figure 8. The phase diagram in the (ρ, T) plane for the potential defined by equation (14). Solid curves $\delta = 0.01\sigma$; dashed curves $\delta = 0.03\sigma$; chain curves $\delta = 0.08\sigma$. The thick curves indicate simulation results, while the thin curves are extrapolation to the exact results at $T = 0$. Density and temperature are in reduced units. Data are from [54].

transition at $\delta \approx 0.25$, a value much larger than for the square-well case. Thus the solid–solid transitions are much more robust for shoulder potentials than for attractive well systems and they may be easier to observe experimentally in colloidal systems with an effective shoulder potential.

In addition to the phase behaviours described above, softened-core potentials may give rise to a phenomenon that is definitely unusual for one-component systems, namely spatial modulations with pattern formation. This takes its origin from the competition between the two repulsive length scales that characterize the potential. The phenomenon was investigated [55, 56] through Monte Carlo simulation in a two-dimensional system of particles interacting through a radially symmetric pair potential which consists of an impenetrable hard core of radius σ plus a repulsive square shoulder extending to $r = \sigma + \delta$. As previously discussed, the effectiveness of each length scale depends on the thermodynamic conditions. At intermediate temperatures and pressures the two distances are both partially effective. This subtle form of competing interactions may yield domain formation.

As shown in figure 9, upon increasing the density, at a fixed temperature, the system rapidly turns from a disordered configuration into a triangular lattice with few defects and lattice constant $\sigma + \delta$. Then, as the shoulder becomes more easily penetrable, particles form dimers together with few short linear chains, that subsequently align in wormlike filaments and eventually form stripe domain patterns similar to those exhibited by 2D real systems [57–59], while at even higher densities, the system is composed mainly of loose aggregates of three or more particles. In contrast to argon-like fluids, where the structure factor $S(k)$ presents at any density and temperature a series of peaks of decreasing height, $S(k)$ shows here an anomalous behaviour: as the density increases, the second peak may become higher than the first and at very high densities (not shown) the third peak becomes the highest one. This behaviour has similarities with that reported for an ultrasoft repulsive potential used to model star polymers [46], and reflects the progressive turning on/off of different effective length scales, signalling the emergence of a new length scale smaller than $\sigma + \delta$ but larger than σ. In the density range where the inner hard core and the external soft corona radii compete with

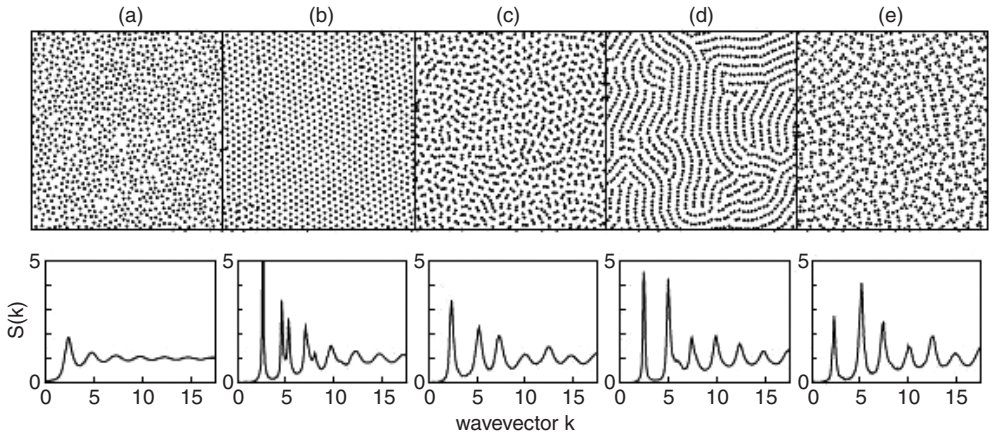

Figure 9. Spatial configuration (top panel) and corresponding structure factors $S(k)$ (bottom panel) for a 2D system interacting through the potential defined by equation (14) with $\delta = 1.5\sigma$. $T = 0.1$: (a) $\rho = 0.1$; (b) $\rho = 0.15$; (c) $\rho = 0.227$; (d) $\rho = 0.291$; (e) $\rho = 0.38$. Quantities are in reduced units: T in units of ε/k_B, ρ in units of $1/\sigma^2$, and wavevector in units of $1/\sigma$. Filled circles represent the hard core of each particle. Data are from [55].

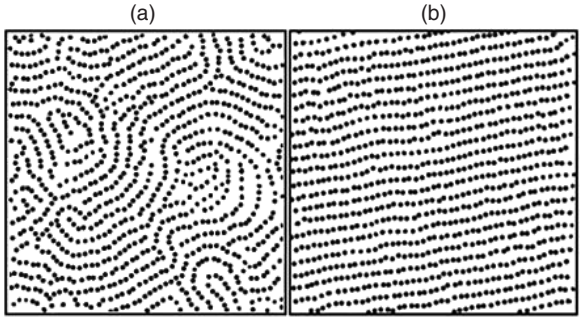

Figure 10. Spatial configuration for a 2D system interacting through the potential defined by equation (14) with $\delta = 1.5\sigma$, immediately above and below the transition to the stripe phase at density $\rho = 0.28$; (a) $T = 0.18$; (b) $T = 0.17$.

each other, decreasing the temperature may induce a transition from a disordered state to an orientationally ordered phase characterized by stripe patterns. By bringing the system, at a fixed density, to low temperature through an accurate annealing procedure, the system undergoes at a temperature T_S a sharp transition from a disordered state to an orientationally ordered phase in which particles are localized along linear domains, consisting in nearly perfectly straight stripes which span the whole system (figure 10). The specific heat at constant volume (proportional to the statistical average of energy fluctuations) shows a neat λ-shaped cusp at T_S. Energy fluctuations thus increase as T_S is approached from above or below, signalling a rearrangement of the spatial ordering around this temperature.

Up to now we have considered purely repulsive shouldered potentials. We will now examine the phase behaviour of potentials with softened core plus an attractive component. These may represent a simplified model for the interactions of substances in which the distance of minimum approach between two molecules depends on their relative orientations, as for

example those characterized by tetrahedral structure such as water, phosphorous, etc. In fact, softened core potentials can be regarded as resulting from an average over the angular part of more realistic potentials, and though representing only a rough approximation, they retain an essential feature of the anisotropic potentials appropriate for H_2O or P, i.e. the existence of two repulsive distances. Whereas in real systems the more or less close interpenetration of two molecules depends on their relative orientation, in softened potential, as previously discussed, it depends on the values of pressure (density) and temperature. In those regimes where both length scales are effective one can expect phenomena typical of more complex anisotropic potentials and related to the competition between expanded and compact structures, such as fluid–fluid transitions, polymorphism, etc. A first-order transition between two liquids of different densities [60] is consistent with experimental data for a variety of materials [61–64], including single-component systems such as water [65–69], silica [70] and carbon [71]. Experimental results [72] indicate that phosphorus can have a high-density liquid (HDL) and a low-density liquid (LDL) phase. Molecular dynamics simulations of specific models for supercooled water [73, 74], liquid carbon [75] and supercooled silica [76] predict the existence of first-order LDL–HDL phase transitions in these substances.

The phase behaviour of a potential with a hard-core repulsion at short distance, a repulsive square shoulder at an intermediate distance, and an attractive square well at long distance, was investigated through molecular dynamics and theoretical means [77–82]. It was found that the system has three fluid phases: gas, low-density liquid (LDL) and high-density liquid (HDL), and the phase diagram shows two first-order fluid–fluid phase transitions ending in a critical point: a gas–LDL and an LDL–HDL critical point (figure 11). No density anomaly $(\partial V/\partial T)_P < 0$ was found; thus the occurrence of two critical points is not necessarily related to such an anomaly. Consequently, the class of systems displaying a second critical point may be broader than previously hypothesized, including systems with no density anomaly. In particular, a second critical point may also exist in liquid metals that can be described by soft-core potentials. The existence of a second critical point, and its stability with respect to crystallization, as well as the relative position of the two critical points, depend crucially on the value of the potential parameters. The phenomenon, in fact, arises from a delicate interplay among the different components of the interaction. The behaviour of the softened-core potential studied is relevant for a number of systems whose interaction may present two repulsive length scales, including colloids, proteins, and liquid metals, which raises the possibility that liquid–liquid phase transitions may be present also in systems where it has not yet been observed. In addition to the square repulsive shoulder discussed above, softened repulsion was also modelled through different functional forms of the potential, as for example a hard core plus a linear repulsive ramp [83, 84]. The results obtained are qualitatively similar to those previously discussed.

Similarly to its purely repulsive counterpart, the hard-sphere–square-shoulder–square-well potential gives rise to pattern formation [56]. The transition to the stripe phase occurs at higher temperatures with respect to the purely repulsive interaction, the general features of the phenomenon being qualitatively unaltered. Attraction then favours alignment of the particles. This can be explained by considering that, at least for sufficiently dense configurations, the presence of attraction gives rise to a sort of line tension which stabilizes the stripes. On the microscopic side, the presence of the attractive well increases the average number of particles in the vicinity of the core which makes possible the penetration of the soft core, and thus the formation of stripes, at significantly higher temperatures. The robustness of stripe formation with respect to attractive forces considerably widens the generality of the addressed phenomenon.

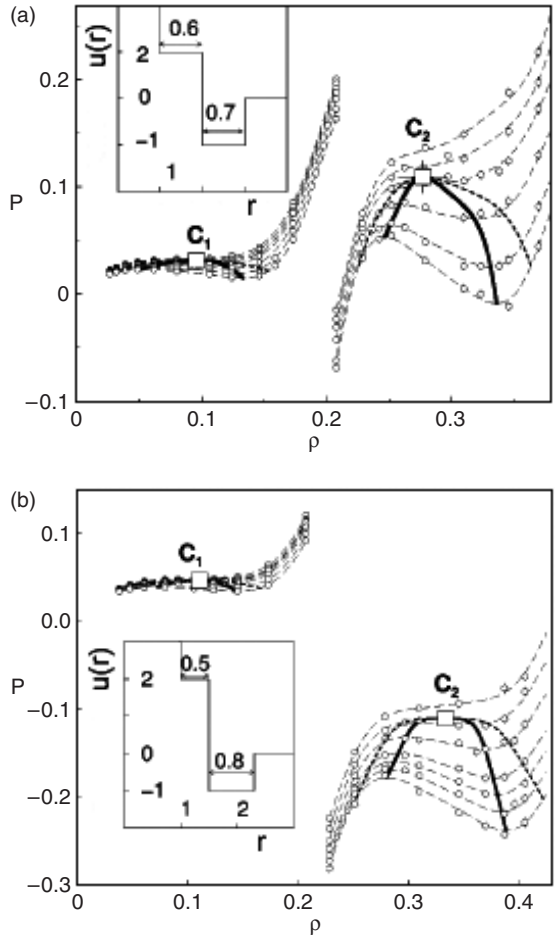

Figure 11. The MD pressure–density phase diagram for the hard-sphere–square-shoulder–square-well potential shown in the inset (the length unit is the hard-core radius while the energy unit is the well depth U_A). Pressure and density are in reduced units. The long-dashed lines are the fits of the calculated state points (circles) at constant temperature. The coexisting regions associated to each spinodal line (bold solid lines) are delimited by the phase transition line (bold dashed line). C_1 and C_2 are the critical points. Panel (a): the isotherms in the low-ρ region (from top to bottom) are for $k_BT/U_A = 1.25, 1.24, 1.23, 1.22, 1.20, 1.18, 1.16$, and in the high-$\rho$ region are for $k_BT/U_A = 0.72, 0.70, 0.68, 0.65, 0.62, 0.60$. Spontaneous crystal nucleation is observed for $T < T_{C_2}$ and $\rho > \rho_{C_2}$. Panel (b): the isotherms (from top to bottom) in the low-ρ region are for $k_BT/U_A = 1.53, 1.52, 1.515, 1.51, 1.50, 1.48, 1.46$, and in the high-$\rho$ region are for $k_BT/U_A = 0.70, 0.68, 0.66, 0.64, 0.63, 0.62, 0.61$. Data are from [81].

4. Bounded repulsion

While it is well assessed that diverging repulsion at close separations between the particles is the dominant factor causing crystallization, one might ask how much repulsion is needed in order to make a solid, a question specular to that, debated in section 2, about how much attraction is needed in order to make a liquid. Though repulsion is necessary to bring about a solidification transition, it may be not sufficient, as in the case of a system interacting through the ultrasoft, logarithmically diverging potential defined by equation (13), which, as discussed in section 3, for a sufficiently small arm number has no solid phase. An even more extreme

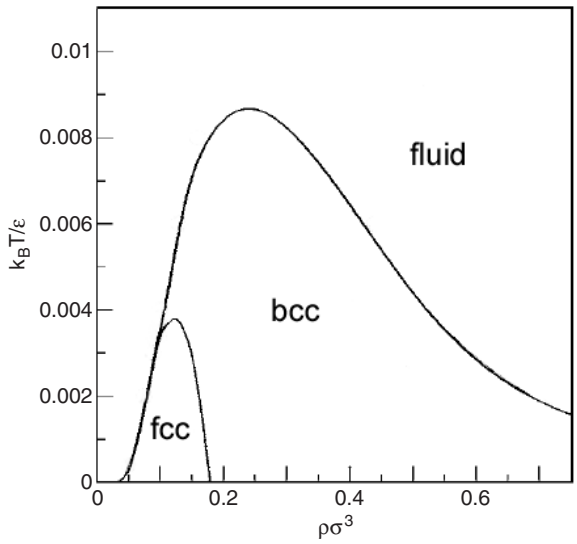

Figure 12. The phase diagram of the Gaussian core model defined by equation (15). The lines mark the stability limit for each homogeneous phase. Data are from [90].

class of potentials is those that model bounded repulsion, and thus remain finite for the whole range of interparticle separations, even at full overlap between the particles [85]. In the context of microscopic interactions in atomic systems, such bounded potentials are unphysical. Due to the harsh repulsion at short distances related to Pauli exclusion principle, a true microscopic interaction always forbids particle overlaps. The situation may be different if one considers interactions among macromolecules. In this case interactions may result in a bounded repulsion that allows the particles to 'sit on top of each other', imposing only a finite energy cost for a full overlap.

Effective interactions between two polymeric coil centroids in a good solvent are characterized by a bounded repulsive interaction that allows two centroids to coincide without this resulting in a forbidden configuration. Such interactions can be described through the Gaussian pair potential [86, 87]:

$$u(r) = \varepsilon e^{-(r/\sigma)^2}, \tag{15}$$

where r is the interparticle distance, ε defines the energy scale, and σ is the length scale. The freezing line of such a system, called the Gaussian core model (GCM), is characterized by the existence of a maximum freezing temperature and a reentrant melting into a dense fluid phase [88–90] (figure 12). Such peculiar behaviour follows from the fact that the penetrability of the Gaussian repulsive core depends crucially on the values of density and temperature. At large temperature and/or density the core is unable to give rise to the excluded volume effects responsible for crystallization, and thus the stable phase is the fluid one. Moreover, the GCM displays a solid–solid phase transition from the fcc to the bcc structure, where the fcc phase is stable at low densities and temperatures. In fact, for small T and ρ the Gaussian repulsion is not easy to penetrate (stiffer repulsion) and the fcc structure is preferred, while at larger T and ρ the core is more easily penetrable (softer repulsion) and the bcc phase is the stable one (see the discussion in section 3). Comparing the phase behaviour of the logarithmic potential described by equation (13) with that of the GCM, one notes that the logarithmic potential, though characterized by a diverging repulsion, has for $f \leqslant 34$ only a fluid phase at all temperatures, while the Gaussian potential exhibits a solid phase at low temperatures. Thus,

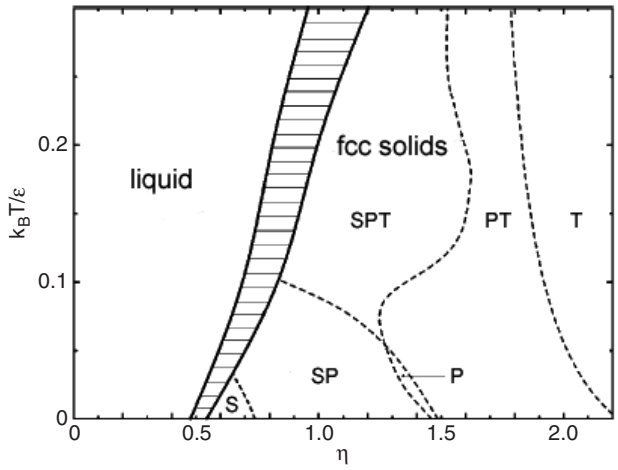

Figure 13. The phase diagram of the penetrable sphere model defined by equation (16). The solid lines denote the first-order liquid–solid freezing transition and the shaded region is the coexistence region. The dashed lines denote second-order clustering transitions between solids differing in the fraction of sites occupied by a single particle (S), pairs (P), triplets (T) (in the S-solid all sites are occupied by a single particle, in the SP solid some sites are occupied by a single particle and the others by pairs, etc). Data are from [92].

a bounded potential may be more effective than a diverging one as far as crystallization is concerned. On the other hand, for $f > 34$, the logarithmic potential displays reentrant melting only for increasing density, whereas the GCM has reentrant melting into the fluid phase both for increasing density and temperature.

A model system apparently simpler than the GCM is the penetrable spheres model (PSM), in which the interaction is a positive, finite constant for separations smaller than a diameter σ, and vanishing otherwise [91]:

$$u(r) = \begin{cases} \varepsilon & r \leqslant \sigma \\ 0 & r > \sigma. \end{cases} \tag{16}$$

The model was studied by means of cell-model calculations and computer simulations [92], liquid-state integral equation theories [93] and density functional theory [94]. It was found that the freezing density of the PSM, that coincides with that of the HS system at $T = 0$ where the two systems become equivalent [85], increases with the temperature at all temperatures (figure 13). Thus, at difference from the GCM, no reentrant melting takes place. This follows from the fact that the solid always lowers its free energy by allowing for multiply occupied crystal sites, a mechanism that is called clustering. The clustering mechanism stabilizes then the solid at all temperatures, and by allowing more and more particles to occupy the same lattice sites, a practically constant effective density of clusters is maintained in the crystal, which leads to a density-independent lattice constant. Freezing from the fluid is followed, by increasing density, by a cascade of second-order clustering transitions in the crystal between solids differing for the fractions of sites occupied by pairs, triplets, etc. When details about the clustering structure of the solid are disregarded, the phase diagram of the PSM and that of potentials with repulsion that diverges, as r approaches zero, at least as $1/r$, are topological similar, the main difference being that in the first case the freezing line exhibits an overall rightward bending, whereas in the latter case it becomes at high temperatures a straight line ($\rho = \text{const}$) parallel to the temperature axis.

The radically different phase behaviour of the GCM and the PSM is somewhat surprising, in the light of the apparent similarity between the two models. The reason for this difference is that whereas in the PSM the particles can build clusters, in the GCM this is not favoured energetically. Recently, a criterion able to establish whether the phase diagram of a system interacting by means of a bounded potential will display clustering or reentrant melting behaviour was derived by employing a mean field-density functional theory [95]. Given a repulsive bounded pair potential which decays quickly enough to zero at large separations, so that it is integrable and its Fourier transform $\phi(q)$ exists, it was shown that if $\phi(q)$ decays monotonically from $\phi(q = 0) = \sigma^{-3} \int \mathrm{d}\vec{r}\, \phi(r) > 0$ to zero for $q \to \infty$, then the phase diagram will display reentrant melting and an upper freezing temperature, otherwise, if $\phi(q)$ decays with an oscillatory behaviour at large q (which occurs for a rapid enough decay of the potential for $r \to \infty$) thus attaining negative values for certain ranges of the wavenumber, the system will freeze at all temperatures, for sufficiently high density. The point was illustrated using a class of bounded potentials, called the Fermi distribution model (FDM) due to its resemblance to the Fermi–Dirac distribution:

$$u(r) = \varepsilon \frac{1 + \mathrm{e}^{-\sigma/\xi}}{1 + \mathrm{e}^{(r-\sigma)/\xi}}, \tag{17}$$

where ξ is a tunable smoothing parameter, and, for all ξ, the potential varies from ε at $r = 0$ to zero at $r \to \infty$. The case $\xi = 0$ recovers the PSM, whereas as ξ grows, the interaction becomes smoother. By using the criterion described above, it was found that members of the FDM with $\xi < \xi_c = 0.496\,97$ display clustering. With increasing ξ, the slope of the high-temperature freezing line decreases, until for $\xi > \xi_c$ the system displays reentrant melting. For $\xi = 0.6$ the phase diagram of the FDM shows a reentrant melting behaviour quite similar to that exhibited by the Gaussian core model.

Due to the constant value of the potential for $r \leqslant \sigma$ and its sharp fall to zero for $r > \sigma$, the PSM is a rather unrealistic model for effective interactions. Clustering was however found to occur also in more realistic potentials. By assembling suitably tailored dendrimers through computer simulation, evidence was found of effective interaction between macromolecules of the type

$$u(r) = \varepsilon \mathrm{e}^{-(r/\sigma)^n}, \tag{18}$$

with $n > 2$. The model described by equation (18), called the generalized exponential model of index n, was recently investigated, through density functional theory [96]. It was shown that $u(r)$ gives rise to reentrant melting for $n \leqslant 2$ (for $n = 2$, the Gaussian core model is recovered), while clustering occurs for $n > 2$ (figure 14). The number of particles participating in a cluster scales linearly with density; therefore the crystals feature density-independent lattice constants. Clustering is accompanied by polymorphic bcc–fcc transition, with fcc being the stable phase at high densities.

5. Conclusions

In recent years the use of effective potentials as a simple way to represent complicate interactions has gained renewed popularity. To a large extent, this is due to the growing relevance of an ample class of substances termed as soft matter. These generally consist in mesoscopic particles with supramolecular architecture largely susceptible to external agents, such as colloidal systems, polymers, and surfactants. An essential feature of soft matter is that it usually offers to the scientist the possibility to tune interactions at a microscopic level. This has considerably enriched the panorama of observable phase phenomena and has enormously widened the range of interaction model potentials having physical relevance. Such potentials,

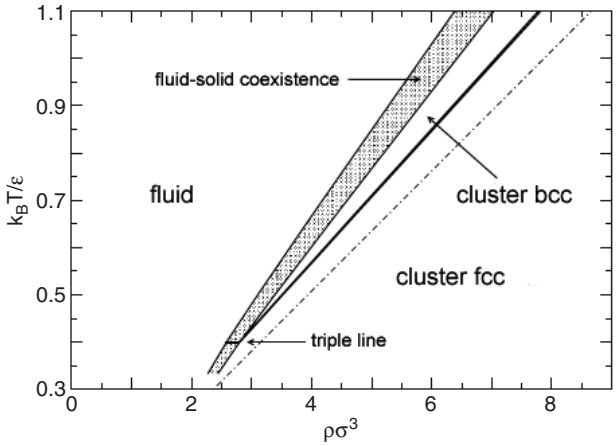

Figure 14. The phase diagram of the generalized exponential model defined by equation (18), with $n = 4$. The shaded area represents the coexistence region of the liquid and the cluster bcc phase. Data are from [96].

when describing interactions among substances characterized by a molecular structure, contain, in a condensed form, informations about the internal degrees of freedom of the macromolecule. Thus, in spite of the simplicity of the functional form that defines the potential dependence on the intermolecular distance, they may give rise to phase behaviours that are radically different from that characterizing typical monoatomic substances.

The concept of intermolecular effective potential has proven useful for an extremely broad range of problems and is essential for much of modern statistical physics. Since this approach is based on approximations that are not always satisfied, it is inadequate for a number of systems. To deal with them, *ab initio* simulations have emerged as an appropriate tool. Though time consuming, these calculations are intrinsically more accurate than those based on effective interactions, and so one might question, with ever-increasing computing power, the usefulness of intermolecular potentials. Undoubtedly, the ability to simulate a phenomenon accurately is invaluable, and may even provide a cheaper alternative to experiment. Reproducing reality is, however, not necessarily tantamount to understanding it. The ability to describe a phenomenon using simple ideas and concepts is the basis for enhanced comprehension [97]. Though the extent to which this is possible varies widely, it remains nonetheless a central goal of scientific investigations. Despite their limitations, intermolecular potentials allow scientists to describe and characterize interactions in terms of just two features, the same that were first pointed out by Empedocles in 500 BC: the universal and eternal dualism of attraction (Love) and repulsion (Strife) [98].

Acknowledgments

The author thanks Professors H Löwen and C Caccamo for a critical reading of the manuscript.

References

[1] Kaplan I G and Rodimova O B 1978 *Sov. Phys.—Usp.* **21** 918
[2] Remler D K and Madden P A 1990 *Mol. Phys.* **70** 921
[3] Hansen J P and McDonald I R 1976 *Theory of Simple Liquids* (London: Academic)

[4] Lennard-Jones J E 1931 *Proc. Camb. Phil. Soc.* **27** 469
[5] van der Waals J D 1880 *Verh. K. Akad. van Wet.* **20** 1–32
van der Waals J D 1880 *Verh. K. Akad. van Wet.* **20** 1–11
[6] Rowlinson J S and van der Waals J D 1988 On the continuity of the gaseous and the liquid states *Studies in Statistical Mechanics* vol XIV, ed J L Lebowitz (Amsterdam: North-Holland)
[7] Pitzer K E 1939 *J. Chem. Phys.* **7** 583
[8] Alder B J and Wainwright T E 1957 *J. Chem. Phys.* **27** 1208
[9] Wood W W and Jacobson J D 1957 *J. Chem. Phys.* **27** 1207
[10] Pusey P N and Van Megen W 1986 *Nature* **320** 340
[11] Bartlett P, Ottewill R H and Pusey P N 1992 *Phys. Rev. Lett.* **68** 3801
[12] Hansen J P and Verlet L 1969 *Phys. Rev.* **184** 151
[13] Gast A P, Hall C K and Russel W B 1983 *J. Colloid Interface Sci.* **96** 251
[14] Asakura S and Oosawa F 1954 *J. Chem. Phys.* **22** 1255
[15] Vrij A 1976 *Pure Appl. Chem.* **48** 471
[16] Russel W B, Saville D A and Schowalter W R 1991 *Colloidal Dispersions* (Cambridge: Cambridge University Press)
[17] Pusey P N 1991 *Liquids, Freezing and Glass Transition* ed J P Hansen, D Levesque and J Zinn-Justin (Amsterdam: North-Holland)
[18] Meijer J and Frenkel D 1991 *Phys. Rev. Lett.* **67** 1110
[19] Lekkerkerker H N W, Poon W C K, Pusey P N, Stroobants A and Warn P B 1992 *Europhys. Lett.* **20** 559
[20] Pusey P N, Poon W C K, Ilett S M and Barlett P 1994 *J. Phys.: Condens. Matter* **6** A29
[21] Calderon L, Bibette J and Biais J 1993 *Europhys. Lett.* **23** 653
[22] Girifalco L A 1992 *J. Phys. Chem.* **96** 858
[23] Hagen M H J, Meijer E J, Mooij G C A M, Frenkel D and Lekkerkerker H N W 1993 *Nature* **365** 425
[24] Cheng A, Klein M L and Caccamo C 1993 *Phys. Rev. Lett.* **71** 1200
[25] Hasegaway M and Ohno K 1997 *J. Phys.: Condens. Matter* **9** 3361
[26] Costa D, Pellicane G, Abramo M C and Caccamo C 2003 *J. Chem. Phys.* **118** 304
[27] Rao A M, Zhou P, Wang J A, Hager G T, Holden J M, Lee W T, Bi X X, Eklund P C, Cornett D S, Duncan M A and Amster I J 1993 *Science* **259** 955
[28] Hagen M H J and Frenkel D 1994 *J. Chem. Phys.* **101** 4093
[29] Tejero C F, Daanoun A, Lekkerkerker H N W and Baus M 1994 *Phys. Rev. Lett.* **73** 752
[30] Baxter R J 1968 *J. Chem. Phys.* **49** 2770
[31] Watts R O, Henderson D and Baxter R J 1971 *Adv. Chem. Phys.* **21** 421
[32] Chiew Y C and Glandt E D 1983 *J. Phys. A: Math. Gen.* **16** 2599
[33] Miller M A and Frenkel D 2004 *J. Chem. Phys.* **121** 535
[34] Liu H, Garde S and Kumar S 2005 *J. Chem. Phys.* **123** 174505
[35] Bolhuis P and Frenkel D 1994 *Phys. Rev. Lett.* **72** 2211
[36] Camp P 2003 *Phys. Rev.* E **67** 011503
[37] Laird B B and Haymet A D J 1992 *Mol. Phys.* **75** 71
[38] Agrawal R and Kofke D A 1995 *Phys. Rev. Lett.* **74** 122
[39] Robbins M O, Kremer K and Grest G S 1988 *J. Chem. Phys.* **88** 3286
[40] Meijer E J and Frenkel D 1991 *J. Chem. Phys.* **94** 2269
[41] Hamaguchi S, Farouki R T and Dubin D H E 1996 *J. Chem. Phys.* **105** 7641
[42] Hamaguchi S, Farouki R T and Dubin D H E 1997 *Phys. Rev.* E **56** 4671
[43] Witten T A, Pincus P A and Cates M E 1986 *Europhys. Lett.* **2** 137
[44] Witten T A and Pincus P A 1986 *Macromolecules* **19** 2509
[45] Likos C N, Löwen H, Watzlawek M, Abbas B, Jucknischke O, Allgaier J and Richter D 1998 *Phys. Rev. Lett.* **80** 4450
[46] Watzlawek M, Likos C N and Löwen H 1999 *Phys. Rev. Lett.* **82** 5289
[47] Stillinger F H and Weber T A 1985 *Phys. Rev.* B **31** 5262
[48] Biswas R and Hamann D R 1985 *Phys. Rev. Lett.* **55** 2001
[49] Tersoff J 1985 *Phys. Rev. Lett.* **56** 632
[50] Hemmer P C and Stell G 1970 *Phys. Rev. Lett.* **24** 1284
[51] Stell G and Hemmer P C 1972 *J. Chem. Phys.* **56** 4274
[52] Young D A and Alder B J 1977 *Phys. Rev. Lett.* **38** 1213
[53] Kincaid J M, Stell G and Goldmark E 1976 *J. Chem. Phys.* **65** 2172
[54] Bolhuis P and Frenkel D 1997 *J. Phys.: Condens. Matter* **9** 381
[55] Malescio G and Pellicane G 2003 *Nat. Mater.* **2** 97

[56] Malescio G and Pellicane G 2004 *Phys. Rev.* E **70** 021202
[57] McConnell G A, Gast A P, Huang J S and Smith S D 1993 *Phys. Rev. Lett.* **71** 2102
[58] Likos C N, Hoffmann N, Löwen H and Louis A 2002 *J. Phys.: Condens. Matter* **14** 7681
[59] Ziherl P and Kamien R D 2000 *Phys. Rev. Lett.* **85** 3528
[60] Debenedetti P G 1998 *Metastable Liquids: Concepts and Principles* (Princeton, NJ: Princeton University Press)
[61] Wilding M C, McMillan P F and Navrotsky A 2001 *J. Cryst. Noncryst. Solids* **293** 357
[62] Brazhkin V V, Popova S V and Voloshin R N 1997 *High Pressure Res.* **15** 267
[63] Brazhkin V, Bulderev S V, Ryzhov V and Stanley H E (ed) 2002 New kinds of phase transitions: transformations in disordered substances *NATO Advanced Research Workshop (Volga River)* vol II/81 (Dordrecht: Kluwer)
[64] Debenedetti P G and Stanley H E 2003 *Phys. Today* **56** 40
[65] Mishima O and Stanley H E 1998 *Nature* **396** 329
[66] Brazhkin V V, Gromnitskaya E L, Stalgorova O V and Lyapin A G 1998 *Rev. High Pressure Sci. Technol.* **7** 1129
[67] Mishima O 2000 *Phys. Rev. Lett.* **85** 334
[68] Bellissent-Funel M C 1998 *Nuovo Cimento* D **20** 2107
[69] Soper A K and Ricci M A 2000 *Phys. Rev. Lett.* **84** 2881
[70] Lacks D J 2000 *Phys. Rev. Lett.* **84** 4629
[71] van Thiel M and Ree F H 1993 *Phys. Rev.* B **48** 3591
[72] Katayama Y, Mizutani T, Utsumi W, Shimomura O, Yamakata M and Funakashi K 2000 *Nature* **403** 170
[73] Poole P H, Sciortino F, Essmann U and Stanley H E 1992 *Nature* **360** 324
[74] Sciortino F, La Nave E and Tartaglia P 2003 *Phys. Rev. Lett.* **91** 155701
[75] Glosli J N and Ree F H 1999 *Phys. Rev. Lett.* **82** 4659
[76] Saika-Voivod I, Sciortino F and Poole P H 2001 *Phys. Rev.* E **63** 011202
[77] Franzese G, Malescio G, Skibinsky A, Bulderev S V and Stanley H E 2001 *Nature* **409** 692
[78] Malescio G and Pellicane G 2001 *Phys. Rev.* E **63** 020501
[79] Franzese G, Malescio G, Skibinsky A, Bulderev S V and Stanley H E 2002 *Phys. Rev.* E **66** 051206
[80] Malescio G, Franzese G, Pellicane G, Skibinsky A, Buldyrev S V and Stanley H E 2002 *J. Phys.: Condens. Matter* **14** 2193
[81] Skibinsky A, Buldyrev S V, Franzese G, Malescio G and Stanley H E 2004 *Phys. Rev.* E **69** 061206
[82] Malescio G, Franzese G, Skibinsky A, Buldyrev S V and Stanley H E 2005 *Phys. Rev.* E **71** 061504
[83] Jagla E A 1999 *J. Chem. Phys.* **111** 8980
[84] Jagla E A 2001 *Phys. Rev.* E **63** 061501
[85] Likos C N 2001 *Phys. Rep.* **348** 267
[86] Stillinger F H 1976 *J. Chem. Phys.* **65** 3968
[87] Stillinger F H and Weber T A 1978 *J. Chem. Phys.* **68** 3837
[88] Stillinger F H and Stillinger D K 1997 *Physica* A **244** 358
[89] Lang A, Likos C N, Watzlawek M and Löwen H 2000 *J. Phys.: Condens. Matter* **12** 5087
[90] Prestipino S, Saija F and Giaquinta P V 2005 *Phys. Rev.* E **71** 050102
[91] Marquest C and Witten T A 1989 *J. Physique* **50** 1267
[92] Likos C N, Watzlawek M and Löwen H 1998 *Phys. Rev.* E **58** 3135
[93] Fernaud M J, Lomba E and Lee L L 2000 *J. Chem. Phys.* **112** 810
[94] Schmidt M 1999 *J. Phys.: Condens. Matter* **11** 10163
[95] Likos C N, Lang A, Watzlawek M and Löwen H 2001 *Phys. Rev.* E **63** 031206
[96] Mladek B M, Gottwald D, Kahl G, Neumann M and Likos C N 2006 *Phys. Rev. Lett.* **96** 045701
[97] Malescio G 2003 *Nat. Mater.* **2** 501
[98] Empedocles 450 BCE circa *On nature* fragments 17, 21, 22, 26